10-9-2018

Electronic structure of the topological superconductor candidate Au2Pb

Yun Wu
Iowa State University and Ames Laboratory, yunw@iastate.edu

Gil Drachuck
Iowa State University and Ames Laboratory

Lin-Lin Wang
Ames Laboratory, llw@ameslab.gov

Duane D. Johnson
Iowa State University and Ames Laboratory, ddj@iastate.edu

Przemyslaw Swatek
Iowa State University and Ames Laboratory

See next page for additional authors

Electronic structure of the topological superconductor candidate Au2Pb

Abstract
We use magnetization measurements, high-resolution angle-resolved photoemission spectroscopy (ARPES), and density functional theory (DFT) calculations to study the electronic properties of Au2Pb, a topological superconductor candidate. The magnetization measurements reveal three discontinuities at 40, 51, and 99 K that agree well with reported structural phase transitions. To measure the band structure along desired crystal orientations, we utilized polishing, sputtering, and annealing to obtain clean flat sample surfaces. ARPES measurements of the Au2Pb (111) surface at 110 K shows a shallow hole pocket at the center and flower-petal-like surface states at the corners of the Brillouin zone. These observations match the results of DFT calculations relatively well. The flower-petal-like surface states appear to originate from a Dirac-like dispersion close to the zone corner. For the Au2Pb(001) surface at 150 K, ARPES reveals at least one electron pocket between the Γ and M points, consistent with the DFT calculations. Our results provide evidence for the possible existence of a Dirac state in this material.

Disciplines
Condensed Matter Physics

Authors
Yun Wu, Gil Drachuck, Lin-Lin Wang, Duane D. Johnson, Przemyslaw Swatek, Benjamin Schrunk, Daixiang Mou, Lunan Huang, Sergey L. Bud'ko, Paul C. Canfield, and Adam Kaminski

Rapid Communications

Electronic structure of the topological superconductor candidate Au_2Pb

Yun Wu,[1,2] Gil Drachuck,[1,2] Lin-Lin Wang,[1] Duane D. Johnson,[1,2,3] Przemyslaw Swatek,[1,2] Benjamin Schrunk,[1,2] Daixiang Mou,[1,2] Lunan Huang,[1,2] S. L. Bud'ko,[1,2] P. C. Canfield,[1,2,*] and Adam Kaminski[1,2,†]

[1]*Division of Materials Science and Engineering, Ames Laboratory, Ames, Iowa 50011, USA*

[2]*Department of Physics and Astronomy, Iowa State University, Ames, Iowa 50011, USA*

[3]*Department of Materials Science and Engineering, Iowa State University, Ames, Iowa 50011, USA*

(Received 2 July 2018; revised manuscript received 13 August 2018; published 9 October 2018)

We use magnetization measurements, high-resolution angle-resolved photoemission spectroscopy (ARPES), and density functional theory (DFT) calculations to study the electronic properties of Au_2Pb, a topological superconductor candidate. The magnetization measurements reveal three discontinuities at 40, 51, and 99 K that agree well with reported structural phase transitions. To measure the band structure along desired crystal orientations, we utilized polishing, sputtering, and annealing to obtain clean flat sample surfaces. ARPES measurements of the Au_2Pb (111) surface at 110 K shows a shallow hole pocket at the center and flower-petal-like surface states at the corners of the Brillouin zone. These observations match the results of DFT calculations relatively well. The flower-petal-like surface states appear to originate from a Dirac-like dispersion close to the zone corner. For the Au_2Pb (001) surface at 150 K, ARPES reveals at least one electron pocket between the Γ and M points, consistent with the DFT calculations. Our results provide evidence for the possible existence of a Dirac state in this material.

DOI: 10.1103/PhysRevB.98.161107

The prediction [1] and observation [2,3] of the Dirac states on the surface of topological insulators have sparked a search for relativistic quasiparticles in condensed matter systems. Dirac fermions have been observed in three-dimensional (3D) Dirac semimetals such as Cd_3As_2 and Na_3Bi [4–6], where the Dirac points are protected by symmetry. By breaking the inversion [7] or time-reversal symmetry [8] in the Dirac fermion systems, Weyl fermion states can be realized. The observation of Fermi-arc surface states, either in type-I [7] or type-II [9–11] Weyl semimetals, has been recognized as one of the distinct signatures of Weyl fermion states. In addition to the Dirac and Weyl fermions, another relativistic quasiparticle, namely, the Majorana fermion, is expected to occur at the intersection of superconductivity and topology.

The Majorana fermion state is fascinating because the quasiparticle is its own antiparticle and the bound state obeys non-Abelian statistics. This distinct feature makes it an excellent candidate for topological quantum computation [12]. One natural platform to realize Majorana fermions is topological superconductors. The topological nature guarantees that the gapless excitations at the surface satisfy the Dirac equation, whereas the superconducting nature guarantees that the particle-hole symmetry leads to indistinguishable particles and antiparticles [13]. There are several routes to realize topological superconductivity [14]. One route is to use the proximity effect [15], such as placing ferromagnetic atomic chains on a superconductor [16]. Another route is to bring superconductivity to topological materials, such as doping the topological insulator Bi_2Se_3 with Cu [17], or applying pressure to Bi_2Se_3 [18]. However, this route suffers from difficulties in crystal synthesis, random distribution of impurities, or in the ease of use for practical applications. A better route is to find stoichiometric single crystals that satisfy both the topological property and superconductivity. Topological nodal line materials [19–21] have Dirac nodes forming a line or arc, among which $PbTaSe_2$ has been reported to show a superconducting transition at $T = 3.7$–3.9 K [22,23]. However, the Majorana fermion states in this material still remain elusive, possibly due to its extreme sensitivity to pressure [23].

Recently, Au_2Pb has attracted attention because of the prediction of a Dirac metal to topological metal transition with a structural phase change [24], while the superconductivity of Au_2Pb has been reported more than 50 years ago [25]. With the topological transition accompanied by a structural phase change, Au_2Pb offers a unique platform for studying the interplay of superconductivity, bulk Dirac states, and topological surface states in one single crystal [24,26]. However, until now, no angle-resolved photoemission spectroscopy (ARPES) measurements have provided direct evidence of topological states in this material.

Here, we present high-resolution ARPES data obtained from (001) and (111) surfaces that were prepared by polishing and undergoing several cycles of *in situ* sputtering and annealing. We collect our ARPES data above 100 K so as to avoid any possible twinning effect associated with the structure transitions (see Fig. 1 below). The Fermi surface on the (111) facet consists of a shallow hole pocket at the Γ point and Fermi-arc-like surface states at the zone corners. On the (001) surface, there is a Dirac-like dispersion with a significant gap between the conduction and valence bands, consistent with the density functional theory (DFT) calculations.

*canfield@ameslab.gov
†kaminski@ameslab.gov

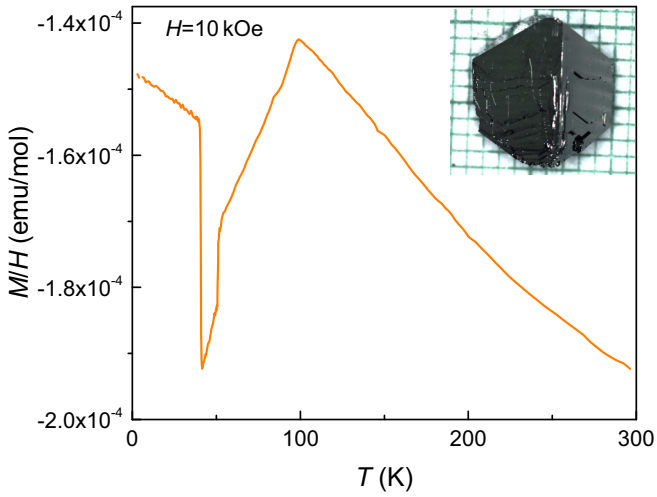

FIG. 1. Temperature-dependent magnetization measurements of Au_2Pb. The inset shows the crystal with naturally grown (111) facets.

Temperature and magnetization measurements were carried out using a Quantum Design magnetic property measurement system (MPMS), superconducting quantum interference device (SQUID) magnetometer ($T = 1.8$–300 K, $H_{max} = 55$ kOe).

Large single-crystalline samples of Au_2Pb were grown out of a high-temperature solution [27,28] rich in Pb. Stoichiometric quantities of elemental Au and Pb were mixed in molar ratios of $Au_{40}Pb_{60}$. The initial elements were placed into the bottom 2-ml alumina crucible of a Canfield crucible set [29], and sealed in amorphous silica ampoules under a partial argon atmosphere. The ampoules were heated to 900 °C in 3 h and dwelled there for 2 h. The ampoules were then rapidly cooled to 410 °C over 3 h, followed by a slow cooling to 280 °C over 150 h. At that point, the excess molten Pb-rich solution was decanted.

Au_2Pb single crystals have naturally grown (111) facets (see the inset to Fig. 1). Flat (001) surfaces of Au_2Pb were obtained by polishing Laue-oriented single crystals. Both surfaces for ARPES measurements were prepared by multiple cycles of annealing the single crystals below the melting point and sputtering in a 10^{-5} Torr argon partial pressure. The ARPES measurements were performed using a helium discharge lamp based ARPES system consisting of a Gamma-data helium ultraviolet lamp and a Scienta SES2002 electron analyzer. The angular and energy resolutions of this system were set at ~0.3° and 15 meV, respectively.

A band structure with spin-orbit (SOC) included has been calculated in DFT [30,31] using the Perdew-Burke-Ernzerhof (PBE) [32] exchange-correlation functional, a plane-wave basis set, and projected augmented-wave method [33] as implemented in VASP [34,35]. For the bulk band structure of Au_2Pb, we used the primitive cell of 6 atoms with a Monkhorst-Pack [36] ($13 \times 13 \times 13$) k-point mesh including the Γ point and a kinetic energy cutoff of 230 eV. For the surface band structure of $Au_2Pb(111)$, a unit cell of 18 atoms with a k-point mesh of ($13 \times 13 \times 3$) is used. Experimental lattice parameters have been used with atoms fixed in their bulk positions. A tight-binding model based on maximally localized Wannier functions [37–39] was constructed to reproduce closely the bulk band structure including SOC in the range of $E_F \pm 1$ eV with Au sd and Pb sp orbitals. Fermi surface and spectral functions of a semi-infinite $Au_2Pb(111)$ surface were calculated with the surface Green's function method [40–43] as implemented in WANNIERTOOLS [44]. Different terminations of the (111) surface have been calculated and we found that the Pb-dimer termination gives the best agreement to ARPES.

Figure 1 shows the temperature-dependent magnetization measurement of a single crystal of Au_2Pb. Three discontinuities are seen at 40, 51, and 99 K, consistent with the previously reported structural phase transitions based on resistivity and specific heat data [24].

Figure 2(a) shows the ARPES intensity integrated within 10 meV about the chemical potential measured on the sputtered and annealed Au_2Pb (111) surface. At the center of both the first and second Brillouin zones (BZs), a shallow hole pocket can be clearly seen. Surrounding the center hole pocket are six flower-petal-like patterns originating from the surface states, which is consistent with the crystal symmetry on this surface. Figure 2(b) shows the calculation of the Au_2Pb (111) surface, which matches relatively well the experimental results. Detailed band structures of Au_2Pb are plotted in Figs. 2(c)–2(j), corresponding to the cuts along No. 1–No. 4 in Fig. 2(a). Through a detailed comparison between the ARPES data and DFT calculations, we can identify those high-intensity bands in ARPES data as surface states. Figure 2(c) shows the band dispersion along cut No. 1 in Fig. 2(a), which is consistent with the surface calculations in Fig. 2(b), especially the parts enclosed by the red and black dashed squares in either figure. The wider band dispersion of the surface states in the experimental data than the DFT calculations can be due to the absence of an ionic relaxation effect in the DFT calculations [45,46]. More details of the flower-petal surface state are shown in Figs. 2(e) and 2(f) along cut No. 2. One can clearly see the surface states emerging from the bulk states and crossing the Fermi level in both the ARPES and surface calculation data, where a possible bulk Dirac dispersion can be identified. The missing parabolic band in ARPES data at $k_2 = 0$ is most likely due to the matrix element effect. For cuts No. 3 and No. 4, the ARPES data and surface calculations show strong consistency except for a 80-meV shift of the chemical potential, probably due to the Pb vacancy defects observed in this material [47].

Figure 3 presents the features observed on the Au_2Pb (111) surface. As shown in Fig. 3(a), the flower-petal surface state seems to terminate and merge into the bulk states. The second derivative of Fig. 3(a) shows that the surface state may terminate before merging into the bulk states, leading to possible Fermi-arc surface states [48]. The Fermi-arc surface state is one of the distinct signatures of Weyl semimetals, which has also been observed in the 3D Dirac semimetal Na_3Bi [49]. Thus, the observation of Fermi-arc-like surface states in Au_2Pb provides evidence for the possible existence of 3D Dirac states, as proposed in Ref. [24]. At higher binding energies, the intensity of the Fermi-surface part enclosed by the red dashed circle in Fig. 3(b) shrinks down to a single point in Fig. 3(c) and expands again to a rough circle in Fig. 3(d). This is consistent with the Dirac-like feature in band dispersion shown in Fig. 3(i) and even better visualized in the second-derivative image shown in Fig. 3(j).

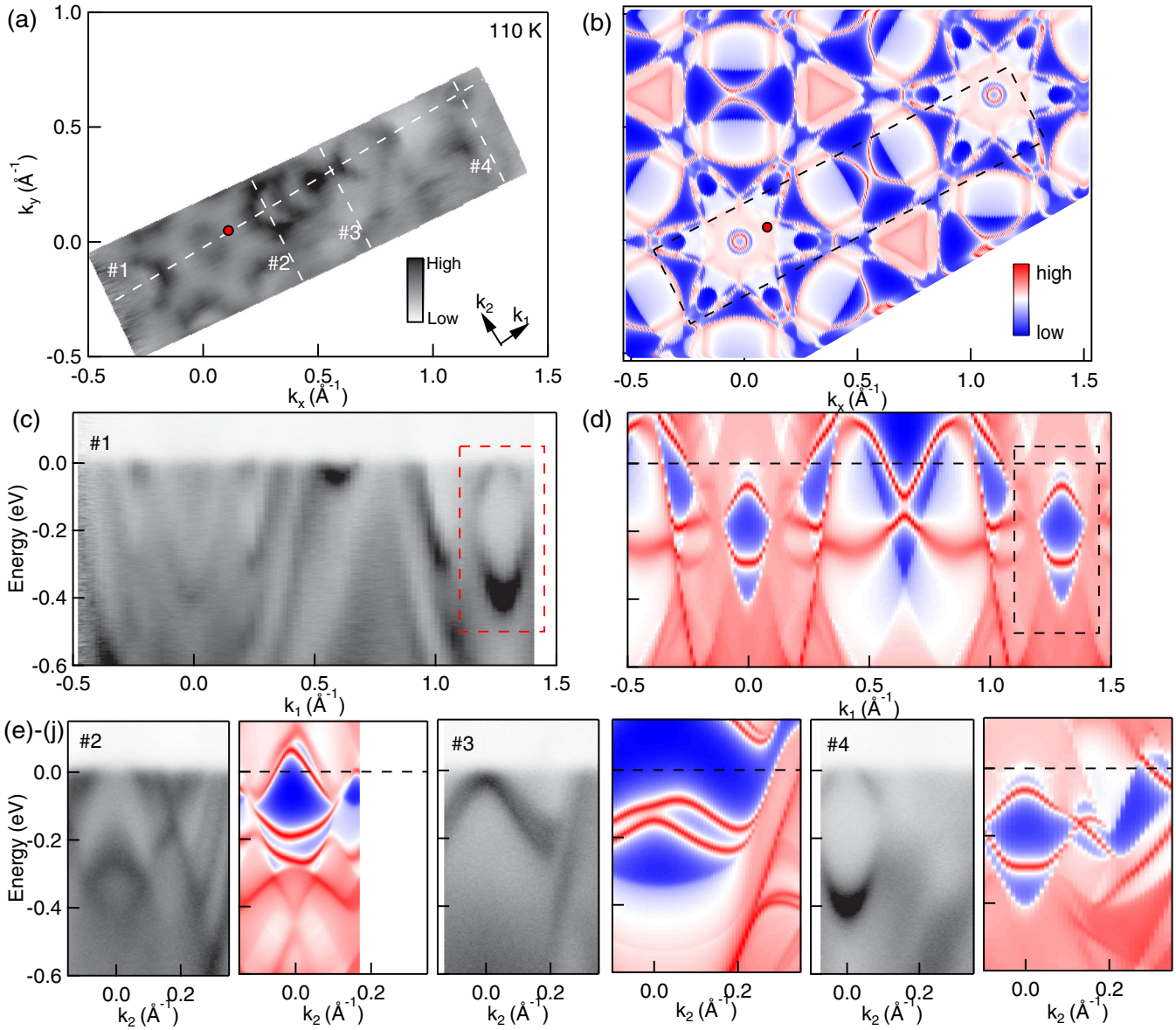

FIG. 2. Fermi surface and band dispersions of the Au_2Pb (111) surface. (a) Fermi-surface plot of ARPES intensity integrated within 10 meV about the chemical potential at 110 K. (b) Calculation of the Au_2Pb (111) surface with Pb-dimer termination at 80 meV below the chemical potential. Note: The red dots in (a) and (b) are shown to provide a reference location of the Dirac point from DFT calculations. The dashed box is the region of data shown in (a). (c)–(j) ARPES intensity and surface band calculations along cuts No. 1–No. 4 in (a). The red and black dashed boxes in (c) and (d) show consistency between ARPES and DFT calculations.

Figure 4 shows the Fermi surface and band dispersion measured on the polished Au_2Pb (001) surface. At almost a quarter way between Γ and *M* points, an electron pocket can be clearly observed. As we further approach the *M* point, another larger pocket can be seen. These observations are consistent with the DFT calculations shown in Fig. 4(b), where the black dashed line encloses the area shown in Fig. 4(a). The band dispersion along the white dashed line in Fig. 4(a) is shown in Fig. 4(c), where a Dirac-like dispersion can be better visualized in its second-derivative image [Fig. 4(d)]. This also matches the result from DFT calculations as shown in Fig. 4(e), except that fewer bands can be observed in the ARPES measurements. This band dispersion also shows a significant gap between the conduction and valence bands, which can be demonstrated by the energy distribution curve (EDC) [Fig. 4(d)] along the red dashed line in Fig. 4(c). A gap size of 200 meV can be estimated by the peak positions in the EDC. Since we only obtained an adequate ARPES intensity at a *k* value off the calculated Dirac point [black solid circle in Fig. 4(b)], we cannot direct approve the existence of the Dirac state in this material. On the other hand, the consistency between the Fermi surface/band dispersion and the band-structure calculations point to the possible existence of a 3D Dirac state on the Au_2Pb (001) surface.

In conclusion, we used magnetization measurements, a high-resolution ARPES system, and DFT calculations to investigate the electronic structure of Au_2Pb single crystals on (111) and (001) surfaces. Three discontinuities can be

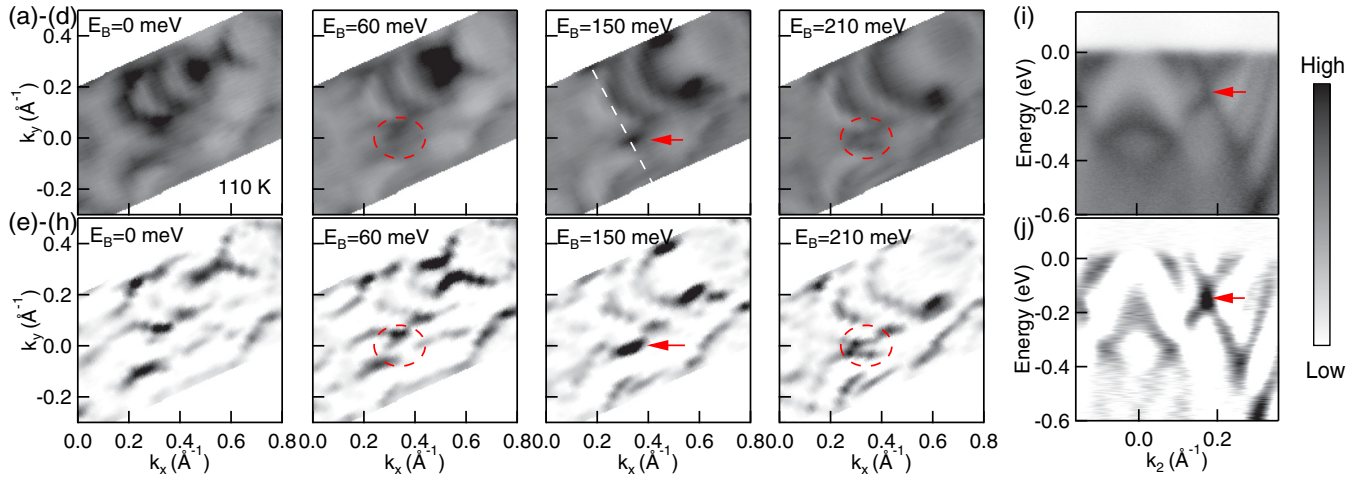

FIG. 3. Constant-energy contours and band dispersion of the Au_2Pb (111) surface measured at 110 K. (a)–(d) ARPES intensity integrated within 10 meV at the binding energies of 0, 60, 150, and 210 meV, respectively. (e)–(h) Second-derivative images of (a)–(d), respectively. (i) Band dispersion along the white dashed line in (c). (j) Second-derivative image of (i). The red dashed circles in (b),(d), (f), and (h) enclose the part of the Dirac-like dispersion. The red arrows in (c), (g), (i), and (j) point to the Dirac-like point.

clearly seen in the magnetization measurements, consistent with the reported structural phase transitions. Interestingly, we observed a Dirac-like dispersion on the polished Au_2Pb (111) surface with Fermi-arc-like surface states. These results are consistent with the surface band-structure calculations. Furthermore, on the Au_2Pb (001) surface, we observed a gapped Dirac-like dispersion. These observations point to the possible topological nature of this material. However, due to the low superconducting transition temperature, we are not able to investigate the potential topological superconductivity in this material. Further study would require better prepared crystal surfaces, and ultralow temperature systems. To conclude, our results and technique to obtain a clean surface on the desired crystal orientations pave the way for

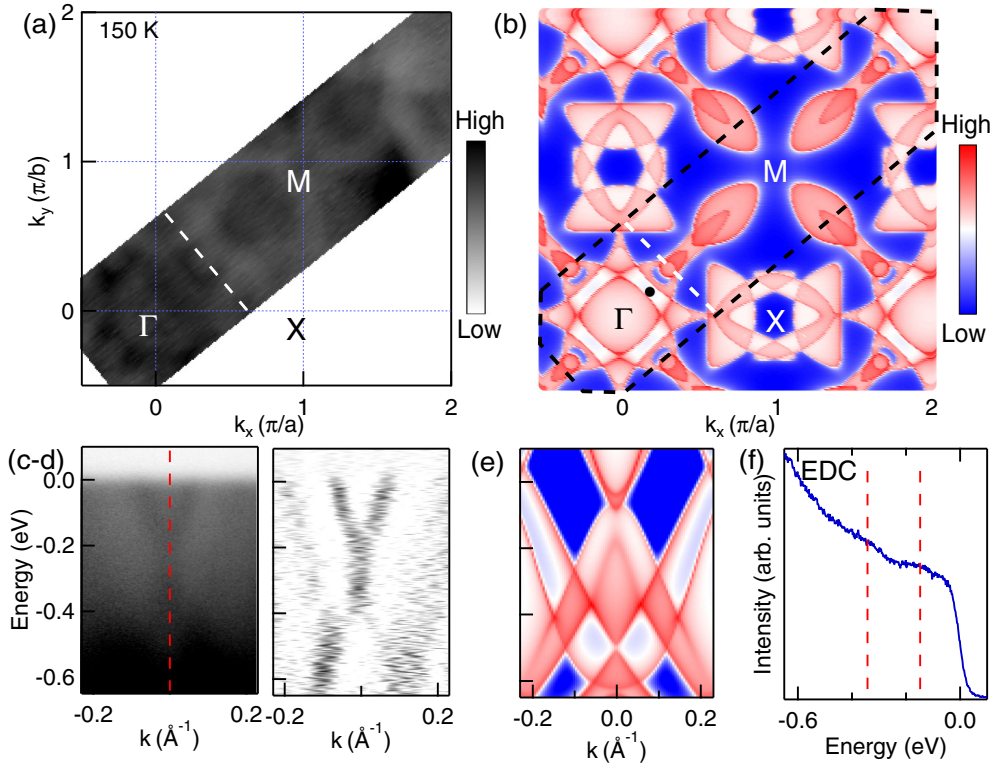

FIG. 4. Fermi surface and band dispersion of Au_2Pb (001) surface measured at 150 K. (a) Fermi-surface plot of ARPES intensity integrated within 10 meV about the chemical potential. (b) Calculated bulk Fermi surface of the Au_2Pb (001) surface. The black dashed line encloses the area of the ARPES measurement in (a). (c) Band dispersion along the white dashed line in (a). (d) Second-derivative image of (c). (e) Calculated band dispersion along the white dashed line in (b). (f) Energy distribution curve (EDC) along the red dashed line in (c).

further exploring the topological superconducting property in this material and make it an ideal candidate for studies of Majorana fermions using scanning tunneling microscopy [16], etc.

Raw data for this Rapid Communication are openly available at the Iowa State University Digital Repository [50].

Research was supported by the U.S. Department of Energy, Office of Basic Energy Sciences, Division of Materials Science and Engineering. Ames Laboratory is operated for the U.S. Department of Energy by Iowa State University under Contract No. DE-AC02-07CH11358. Y.W. and L.L.W. were partially supported by Ames Laboratory's Laboratory-Directed Research and Development (LDRD) funding. G.D. was supported by the Gordon and Betty Moore Foundation EPiQS Initiative (Grant No. GBMF4411). B.S. and L.H. were supported by CEM, a NSF MRSEC, under Grant No. DMR-1420451.

[1] H. Zhang, C.-X. Liu, X.-L. Qi, X. Dai, Z. Fang, and S.-C. Zhang, Nat. Phys. **5**, 438 (2009).
[2] Y. Xia, D. Qian, D. Hsieh, L. Wray, A. Pal, H. Lin, A. Bansil, D. Grauer, Y. S. Hor, R. J. Cava, and M. Z. Hasan, Nat. Phys. **5**, 398 (2009).
[3] Y. L. Chen, J. G. Analytis, J.-H. Chu, Z. K. Liu, S.-K. Mo, X. L. Qi, H. J. Zhang, D. H. Lu, X. Dai, Z. Fang, S. C. Zhang, I. R. Fisher, Z. Hussain, and Z.-X. Shen, Science **325**, 178 (2009).
[4] Z. K. Liu, B. Zhou, Y. Zhang, Z. J. Wang, H. M. Weng, D. Prabhakaran, S.-K. Mo, Z. X. Shen, Z. Fang, X. Dai, Z. Hussain, and Y. L. Chen, Science **343**, 864 (2014).
[5] M. Neupane, S. Xu, R. Sankar, N. Alidoust, G. Bian, C. Liu, I. Belopolski, T. Chang, H. Jeng, H. Lin, A. Bansil, F. Chou, and M. Z. Hasan, Nat. Commun. **5**, 3786 (2014).
[6] Z. K. Liu, J. Jiang, B. Zhou, Z. J. Wang, Y. Zhang, H. M. Weng, D. Prabhakaran, S.-K. Mo, H. Peng, P. Dudin, T. Kim, M. Hoesch, Z. Fang, X. Dai, Z. X. Shen, D. L. Feng, Z. Hussain, and Y. L. Chen, Nat. Mater. **13**, 677 (2014).
[7] S.-Y. Xu, I. Belopolski, N. Alidoust, M. Neupane, G. Bian, C. Zhang, R. Sankar, G. Chang, Z. Yuan, C.-C. Lee, S.-M. Huang, H. Zheng, J. Ma, D. S. Sanchez, B. Wang, A. Bansil, F. Chou, P. P. Shibayev, H. Lin, S. Jia, and M. Z. Hasan, Science **349**, 613 (2015).
[8] Z. Wang, M. G. Vergniory, S. Kushwaha, M. Hirschberger, E. V. Chulkov, A. Ernst, N. P. Ong, R. J. Cava, and B. A. Bernevig, Phys. Rev. Lett. **117**, 236401 (2016).
[9] L. Huang, T. M. McCormick, M. Ochi, Z. Zhao, M. Suzuki, R. Arita, Y. Wu, D. Mou, H. Cao, J. Yan, N. Trivedi, and A. Kaminski, Nat. Mater. **15**, 1155 (2016).
[10] A. Tamai, Q. S. Wu, I. Cucchi, F. Y. Bruno, S. Riccò, T. K. Kim, M. Hoesch, C. Barreteau, E. Giannini, C. Besnard, A. A. Soluyanov, and F. Baumberger, Phys. Rev. X **6**, 031021 (2016).
[11] K. Deng, G. Wan, P. Deng, K. Zhang, S. Ding, E. Wang, M. Yan, H. Huang, H. Zhang, Z. Xu, J. Denlinger, A. Fedorov, H. Yang, W. Duan, H. Yao, Y. Wu, S. Fan, H. Zhang, X. Chen, and S. Zhou, Nat. Phys. **12**, 1105 (2016).
[12] C. Nayak, S. H. Simon, A. Stern, M. Freedman, and S. Das Sarma, Rev. Mod. Phys. **80**, 1083 (2008).
[13] M. Sato and Y. Ando, Rep. Prog. Phys. **80**, 076501 (2017).
[14] C. Beenakker and L. Kouwenhoven, Nat. Phys. **12**, 618 (2016).
[15] L. Fu and C. L. Kane, Phys. Rev. Lett. **100**, 096407 (2008).
[16] S. Nadj-Perge, I. K. Drozdov, J. Li, H. Chen, S. Jeon, J. Seo, A. H. MacDonald, B. A. Bernevig, and A. Yazdani, Science **346**, 602 (2014).
[17] Y. S. Hor, A. J. Williams, J. G. Checkelsky, P. Roushan, J. Seo, Q. Xu, H. W. Zandbergen, A. Yazdani, N. P. Ong, and R. J. Cava, Phys. Rev. Lett. **104**, 057001 (2010).
[18] K. Kirshenbaum, P. S. Syers, A. P. Hope, N. P. Butch, J. R. Jeffries, S. T. Weir, J. J. Hamlin, M. B. Maple, Y. K. Vohra, and J. Paglione, Phys. Rev. Lett. **111**, 087001 (2013).
[19] G. Bian, T. Chang, R. Sankar, S. Xu, H. Zheng, T. Neupert, C. Chiu, S. Huang, G. Chang, I. Belopolski, D. S. Sanchez, M. Neupane, N. Alidoust, C. Liu, B. Wang, C. Lee, H. Jeng, C. Zhang, Z. Yuan, S. Jia *et al.*, Nat. Commun. **7**, 10556 (2016).
[20] Y. Wu, L. Wang, E. Mun, D. D. Johnson, D. Mou, L. Huang, Y. Lee, S. L. Bud'ko, P. C. Canfield, and A. Kaminski, Nat. Phys. **12**, 667 (2016).
[21] L. M. Schoop, M. N. Ali, C. Straszer, A. Topp, A. Varykhalov, D. Marchenko, V. Duppel, S. S. P. Parkin, B. V. Lotsch, and C. R. Ast, Nat. Commun. **7**, 11696 (2016).
[22] M. N. Ali, Q. D. Gibson, T. Klimczuk, and R. J. Cava, Phys. Rev. B **89**, 020505 (2014).
[23] U. S. Kaluarachchi, Y. Deng, M. F. Besser, K. Sun, L. Zhou, M. C. Nguyen, Z. Yuan, C. Zhang, J. S. Schilling, M. J. Kramer, S. Jia, C.-Z. Wang, K.-M. Ho, P. C. Canfield, and S. L. Bud'ko, Phys. Rev. B **95**, 224508 (2017).
[24] L. M. Schoop, L. S. Xie, R. Chen, Q. D. Gibson, S. H. Lapidus, I. Kimchi, M. Hirschberger, N. Haldolaarachchige, M. N. Ali, C. A. Belvin, T. Liang, J. B. Neaton, N. P. Ong, A. Vishwanath, and R. J. Cava, Phys. Rev. B **91**, 214517 (2015).
[25] D. Hamilton, C. Raub, B. Matthias, E. Corenzwit, and G. Hull, J. Phys. Chem. Solids **26**, 665 (1965).
[26] Y. Xing, H. Wang, C. Li, X. Zhang, J. Liu, Y. Zhang, J. Luo, Z. Wang, Y. Wang, L. Ling, M. Tian, S. Jia, J. Feng, X. Liu, J. Wei, and J. Wang, npj Quantum Mater. **1**, 16005 (2016).
[27] P. C. Canfield and I. R. Fisher, J. Cryst. Growth **225**, 155 (2001).
[28] P. C. Canfield and Z. Fisk, Philos. Mag. B **65**, 1117 (1992).
[29] P. C. Canfield, T. Kong, U. S. Kaluarachchi, and N. H. Jo, Philos. Mag. **96**, 84 (2016).
[30] P. Hohenberg and W. Kohn, Phys. Rev. **136**, B864 (1964).
[31] W. Kohn and L. J. Sham, Phys. Rev. **140**, A1133 (1965).
[32] J. P. Perdew, K. Burke, and M. Ernzerhof, Phys. Rev. Lett. **77**, 3865 (1996).
[33] P. E. Blöchl, Phys. Rev. B **50**, 17953 (1994).
[34] G. Kresse and J. Furthmüller, Phys. Rev. B **54**, 11169 (1996).
[35] G. Kresse and J. Furthmüller, Comput. Mater. Sci. **6**, 15 (1996).
[36] H. J. Monkhorst and J. D. Pack, Phys. Rev. B **13**, 5188 (1976).
[37] N. Marzari and D. Vanderbilt, Phys. Rev. B **56**, 12847 (1997).
[38] I. Souza, N. Marzari, and D. Vanderbilt, Phys. Rev. B **65**, 035109 (2001).
[39] N. Marzari, A. A. Mostofi, J. R. Yates, I. Souza, and D. Vanderbilt, Rev. Mod. Phys. **84**, 1419 (2012).
[40] D. H. Lee and J. D. Joannopoulos, Phys. Rev. B **23**, 4988 (1981).

[41] D. H. Lee and J. D. Joannopoulos, Phys. Rev. B **23**, 4997 (1981).
[42] M. P. L. Sancho, J. M. L. Sancho, and J. Rubio, J. Phys. F: Met. Phys. **14**, 1205 (1984).
[43] M. P. L. Sancho, J. M. L. Sancho, J. M. L. Sancho, and J. Rubio, J. Phys. F: Met. Phys. **15**, 851 (1985).
[44] Q. Wu, S. Zhang, H.-F. Song, M. Troyer, and A. A. Soluyanov, Comput. Phys. Commun. **224**, 405 (2018).
[45] N. Fukui, T. Hirahara, T. Shirasawa, T. Takahashi, K. Kobayashi, and S. Hasegawa, Phys. Rev. B **85**, 115426 (2012).
[46] M. V. Kuznetsov, L. V. Yashina, J. Sánchez-Barriga, I. I. Ogorodnikov, A. S. Vorokh, A. A. Volykhov, R. J. Koch, V. S. Neudachina, M. E. Tamm, A. P. Sirotina, A. Y. Varykhalov, G. Springholz, G. Bauer, J. D. Riley, and O. Rader, Phys. Rev. B **91**, 085402 (2015).
[47] K. W. Chen, D. Graf, T. Besara, A. Gallagher, N. Kikugawa, L. Balicas, T. Siegrist, A. Shekhter, and R. E. Baumbach, Phys. Rev. B **93**, 045118 (2016).
[48] I. Belopolski, S.-Y. Xu, D. S. Sanchez, G. Chang, C. Guo, M. Neupane, H. Zheng, C.-C. Lee, S.-M. Huang, G. Bian, N. Alidoust, T.-R. Chang, B. K. Wang, X. Zhang, A. Bansil, H.-T. Jeng, H. Lin, S. Jia, and M. Z. Hasan, Phys. Rev. Lett. **116**, 066802 (2016).
[49] S.-Y. Xu, C. Liu, S. K. Kushwaha, R. Sankar, J. W. Krizan, I. Belopolski, M. Neupane, G. Bian, N. Alidoust, T.-R. Chang, H.-T. Jeng, C.-Y. Huang, W.-F. Tsai, H. Lin, P. P. Shibayev, F.-C. Chou, R. J. Cava, and M. Z. Hasan, Science **347**, 294 (2015).
[50] Y. Wu, G. Drachuck, L.-L. Wang, D. D. Johnson, P. Swatek, B. Schrunk, D. Mou, L. Huang, S. L. Bud'ko, P. C. Canfield, and A. Kaminski, http://lib.dr.iastate.edu/ameslab_datasets/.